nature geoscience

SUPPLEMENTARY INFORMATION

DOI: 10.1038/NGEO1450

# Slight mass gain of Karakoram glaciers in the early twenty-first century

Julie Gardelle[1], Etienne Berthier[2] and Yves Arnaud[3]

[1] *CNRS - Université Grenoble 1, LGGE UMR 5183, 54 rue Molière, Domaine Universitaire, BP 96, 38402 Saint Martin d'Hères Cedex, France*

[2] *CNRS, Université de Toulouse, LEGOS, 14 av. Edouard Belin, Toulouse 31400, France*

[3] *IRD – Université Grenoble 1, LTHE UMR 5564/LGGE UMR 5183, 54 rue Molière, Domaine Universitaire, BP 96, 38402 Saint Martin d'Hères Cedex, France*

In this document, we provide additional information on the digital elevation models (DEMs) used to compute the mass balance over the study area, as well as on glacier delineation and regional ELA determination.

We also explain how surface ablations rates were inferred from thinning rates on Khurdopin Glacier (Fig. S1).

The error analysis is also described and the impact of the successive DEMs corrections are given in Tab. S1. The distribution and spatial pattern of elevation differences off glaciers are shown in Fig. S4 and S5 and the elevation changes on glaciers displayed in Fig. S2 and S6. The extent of the area used to estimate the sea-level contribution of Karakoram glaciers is shown in Fig. S3.

## Satellite DEMs

The more recent DEM is derived from a pair of stereoscopic images acquired 3 December 2008 by the HRS sensor onboard the SPOT5 satellite[31] (Fig. 1). The earlier topography was generated by interferometric processing of C-Band SAR images acquired during the SRTM mission in February 2000 (ref. 32). The SRTM DEM and the mask showing the pixels where data voids were filled by interpolation, originally at a 3 arc sec resolution (~90 m), are resampled to 40 m (UTM zone 43N, ellipsoid WGS84) to match the projection and the posting of the SPOT5 DEM. Altitudes are defined above the EGM96 geoid for both DEMs.

## Glacier delineation and regional ELA

The glacier outlines are derived from a LANDSAT TM image from 29 August 1998. Clean ice and snow areas are detected automatically by applying a threshold to the Normalised Difference Snow Index (TM2 – TM5)/(TM2 + TM5). Debris-covered parts were digitized manually by visual interpretation. The total glacier area is 5,615 km², including 1,460 km² of surge-type glaciers. Between 1998 and 2008, the region experienced minor changes in glacierized area except for a few glaciers that surged and advanced. For the latter, their front positions have been updated manually based on the 3 December 2008 SPOT5 image.

In order to perform an adequate volume to mass conversion, we determined the mean regional equilibrium-line altitude to distinguish between accumulation and ablation areas. As the 29 August 1998 LANDSAT image is cloud free and was acquired near the end of the ablation season (with minimal snow-cover), the observed snowlines can be considered as a first approximation of the equilibrium lines[33]. Therefore, we manually digitized the snowlines for a subsample of 36 non-surging glaciers and computed their mean elevation (ca 5000 m).

## Ablation rates on Khurdopin Glacier

The presence in our study area of glaciers in the quiescent phase of the surge cycle provides an opportunity to infer area-average ablation rates for debris-covered glacier tongues. In particular, Khurdopin Glacier ended its most recent surge in 1999 (ref. 10), before the acquisition of the SRTM DEM. Thus, during 2000-2008, this glacier was nearly stagnant and experienced rapid surface lowering (Figs 2 and 3). For a non-flowing glacier, the ice flux term

can be neglected in the continuity equation and, thus, the surface elevation change equals the surface mass balance[34]. We verify the assumption of glacier stagnation by tracking features on 4 pairs of coregistered LANDSAT and ASTER images acquired between 2000 and 2008 (ref. 35). Cross-sectional mean surface velocities of 9.9 ± 1.8 m $a^{-1}$ were measured at a 1.3 km wide flux gate (draining 130 km² of glacier) located just upstream of the area where the ablation rates are estimated (Fig. S1). We cannot estimate ice fluxes because the bedrock topography is unknown for this remote glacier. Thus, the ablation rates reported below are minimum estimates and would increase linearly by about 0.2 m $a^{-1}$ w.e. for every 100 m increment in the cross-sectional mean ice thickness. For a 6.1 km² mostly debris-covered area in the lower reaches of Khurdopin Glacier (Fig. S1), we inferred an ablation rate of 6.2 m $a^{-1}$ w.e. This ablation rate is high but not uncommon for debris-covered tongues. For example, Nuimura *et al.*[36] inferred just slightly lower ablation rates (5 to 6 m $a^{-1}$ w.e.) by applying mass conservation to the tongue of Khumbu Glacier (Nepal). The high tongue-wide ablation rates measured here on a debris-covered tongue may be due to factors that enhance ice melt, such as (i) the fact that some glacier parts are only covered with a thin layer of debris[16,37], (ii) the existence of melt-water ponds at the glacier surface[19] and (iii) the enhanced ablation at ice cliffs[38].

**GRACE data analysis**

GRACE-derived satellite gravity fields have been recently used to assess glacier loss over central Asia. Matsuo and Heki[39] reported a mass loss rate of 47 ± 12 Gt $yr^{-1}$ for the high mountains of Asia between 2003 and 2009 whereas Jacob *et al.*[40] found for the same region a loss rate of 4 ± 20 Gt $yr^{-1}$ for 2003-2010. Given the large and, to our knowledge, unexplained discrepancies between those two studies, we prefer not to compare our results to GRACE, especially since no value is given by Jacob *et al.*[40] for Karakoram only (they found a mass loss rate of -5 ± 6 Gt $yr^{-1}$ over a large region that includes both Karakoram and Himalaya).

**Error analysis**

The mean elevation change $\Delta h$ of each altitude range is computed with its corresponding standard deviation $\sigma_{\Delta h}$. We assume that the uncertainty $E_{\Delta hi}$ of a single pixel elevation change is equal to the standard deviation $\sigma_{\Delta h}$ of the altitude range it belongs to. This assumption is

rather conservative. $\sigma_{\Delta h}$ includes both measurement uncertainty and real variations of elevation changes within the altitude interval such that the actual elevation change uncertainty of a single pixel is certainly lower than this value. This is confirmed by the fact that the standard deviation of the elevation differences off glaciers (8 m, Fig. S6) is smaller than on glaciers (ranging from 8 to 15 m for the different altitude ranges).

As elevation changes are averaged within 100 m altitude ranges, the resulting error $E_{\Delta h}$ on $\Delta h$ is reduced according to the square root of the number of spatially independent measurements ($N_{eff}$) in the altitude interval:

$$E_{\Delta h} = \frac{E_{\Delta hi}}{\sqrt{N_{eff}}} \qquad (1)$$

$N_{eff}$ is computed for each altitude interval, given the total number of pixels $N_{tot}$ used to calculate the mean $\Delta h$, and the distance of spatial autocorrelation $d$, expressed in pixels[41]:

$$N_{eff} = \frac{N_{tot}}{2d} \qquad (2)$$

$d$ is determined using Moran's I autocorrelation index[42] computed off glaciers and is found to be 18 pixels (i.e. 720 m). Thus, $N_{eff}$ is less than $N_{tot}$ by a factor of 0.03. For non-surging glaciers, $N_{tot}$ ranges from 200 to 115000 pixels, depending on the elevation-band considered.

The error on the SRTM penetration correction is computed as explained above but with $\Delta h$ standing for elevation differences between SRTM X-band and C-band DEMs.

Regarding the seasonality correction (i.e. estimation of the accumulation between early December 1999 and mid-February 2000), we estimate a conservative 100% error (±0.26 m w.e.) on the accumulation rate, as it was measured on a single glacier (Biafo) for the 1985-86 glaciological year, that is not included in our study period[30].

The uncertainties for the regional mass balances are:

± 0.09 m $a^{-1}$ w.e. for the 2000-2008 elevation difference

± 0.17 m $a^{-1}$ w.e. for the SRTM penetration

± 0.03 m $a^{-1}$ w.e. for the seasonality correction

The final uncertainty on our mass balance estimate is then calculated according to standard principles of error propagation.

**Table S1:** Impact and values of successive additive corrections on the region-wide annual mass balance (B). Corrections are applied successively from left to right and are described in the Methods section.

| | | **Planimetric adjustment** | | **Along/Across track correction** | | **Curvature correction** | | **Penetration correction** | |
|---|---|---|---|---|---|---|---|---|---|
| **B ($m\ a^{-1}$ w.e.)** | +0.46 | | +0.44 | | +0.29 | | +0.40 | | +0.11 |
| **Correction ($m\ a^{-1}$ w.e.)** | | -0.02 | | -0.15 | | +0.11 | | -0.29 | |

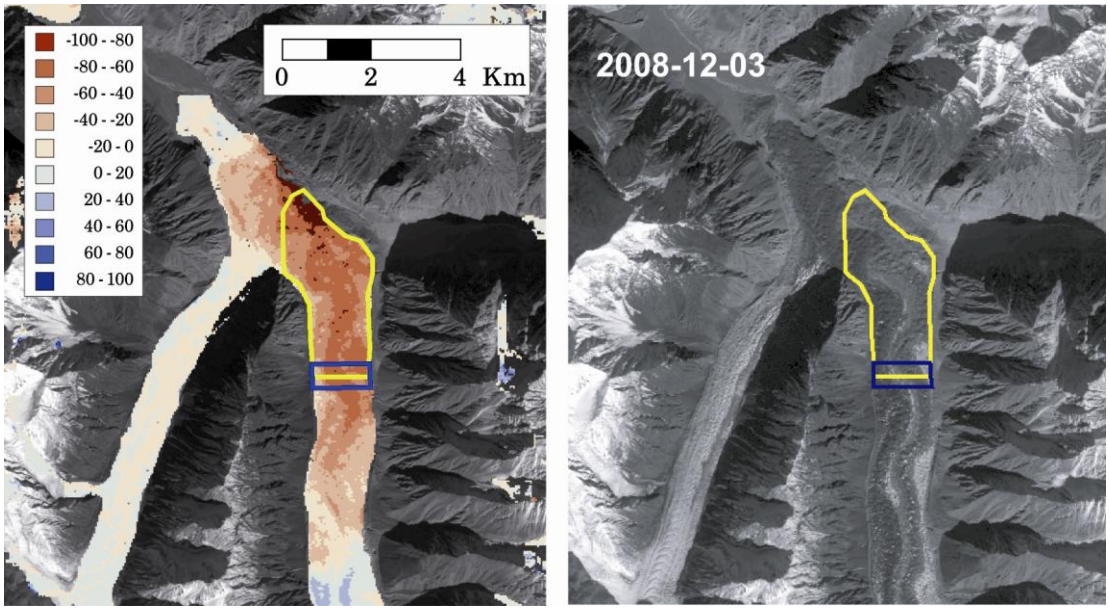


**Figure S1:** Elevation changes (m) and satellite image of the lower Khurdopin Glacier, a surge-type glacier in a quiescent phase during 2000-2008. Left panel: map of ice elevation changes (m) during 2000-2008. The blue box locates the flux gate where the mean 2000-2008 velocity is measured. The yellow polygon shows the area where the thinning rate (and thus the ablation rate) is averaged. Right panel: SPOT5-HRS image acquired 3 December 2008 (© CNES 2008 / Distribution Spot Image).

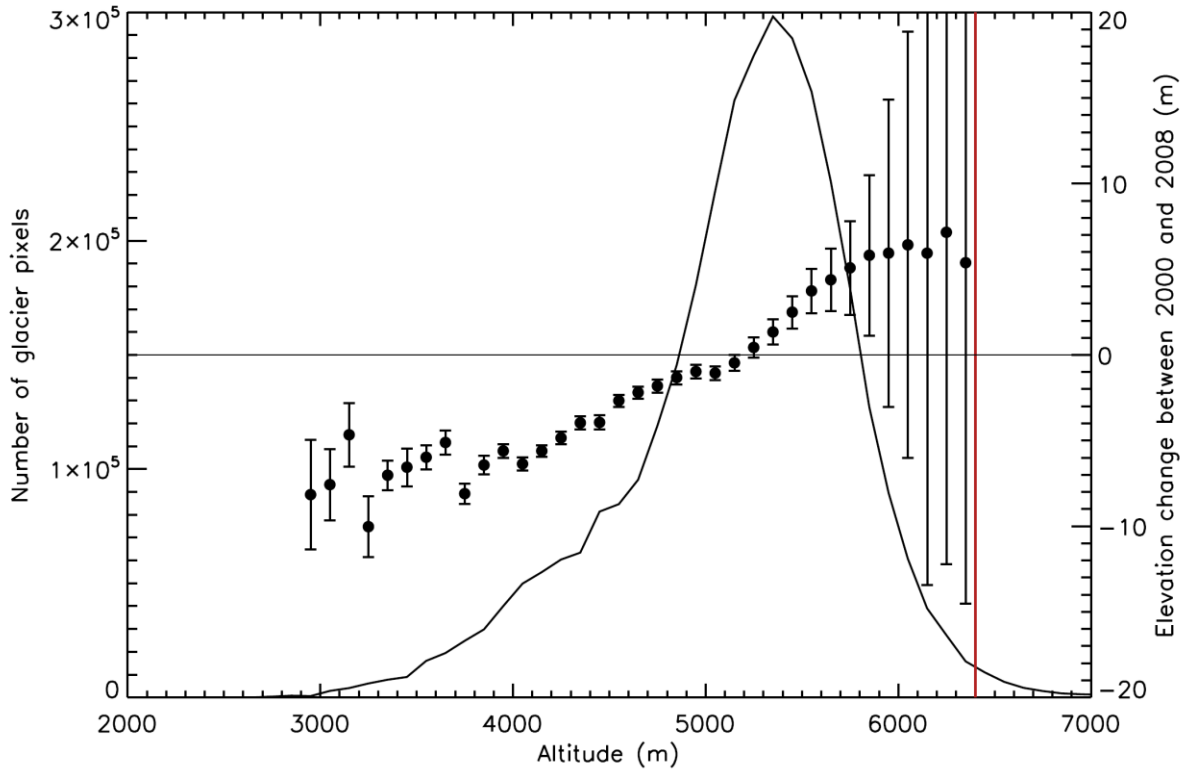


**Figure S2:** Distribution of all ice-covered area (including surge-type glaciers) as a function of altitude (black curve, left vertical axis) and elevation changes over non surging glaciers (black circles, right vertical axis) with their error bars. No reliable elevation changes measurements could be performed above 6400 m a.s.l. (shown by a vertical red line).

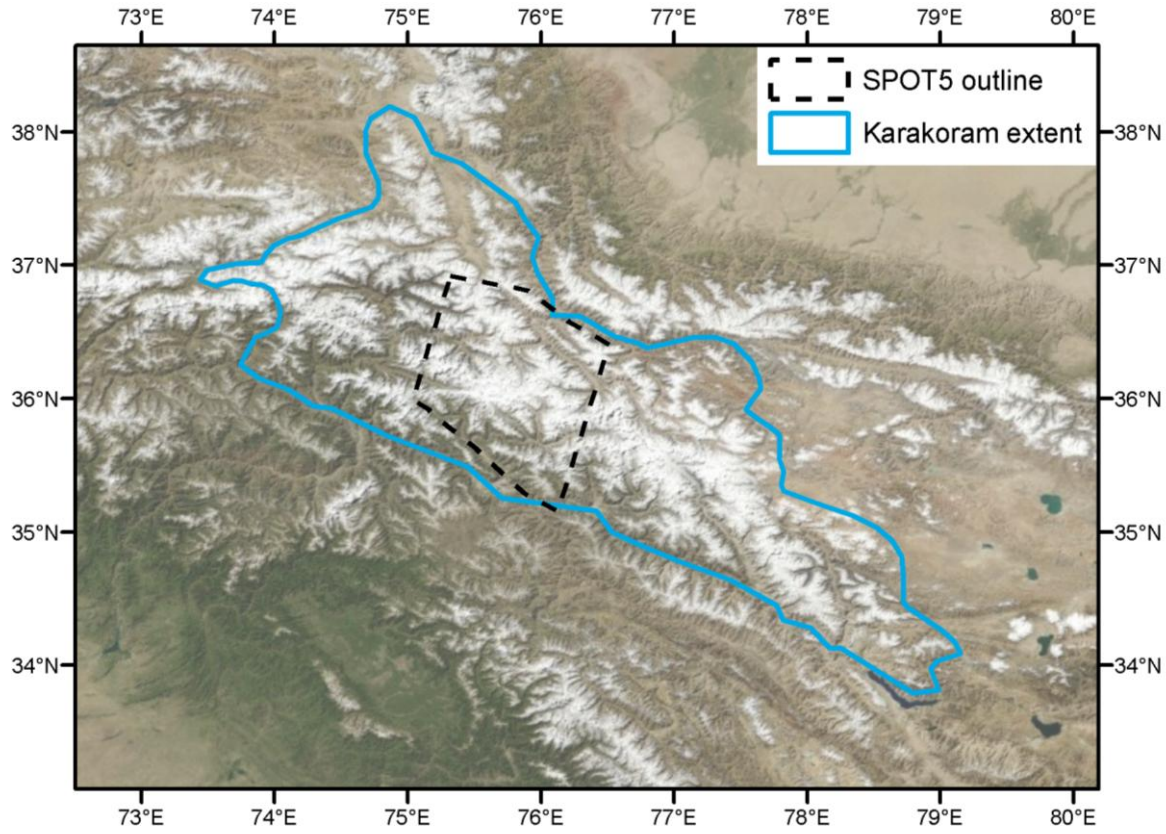


**Figure S3:** Extent of the Karakoram region used in this study to calculate the sea level contribution (background image: © NASA's Earth Observatory).

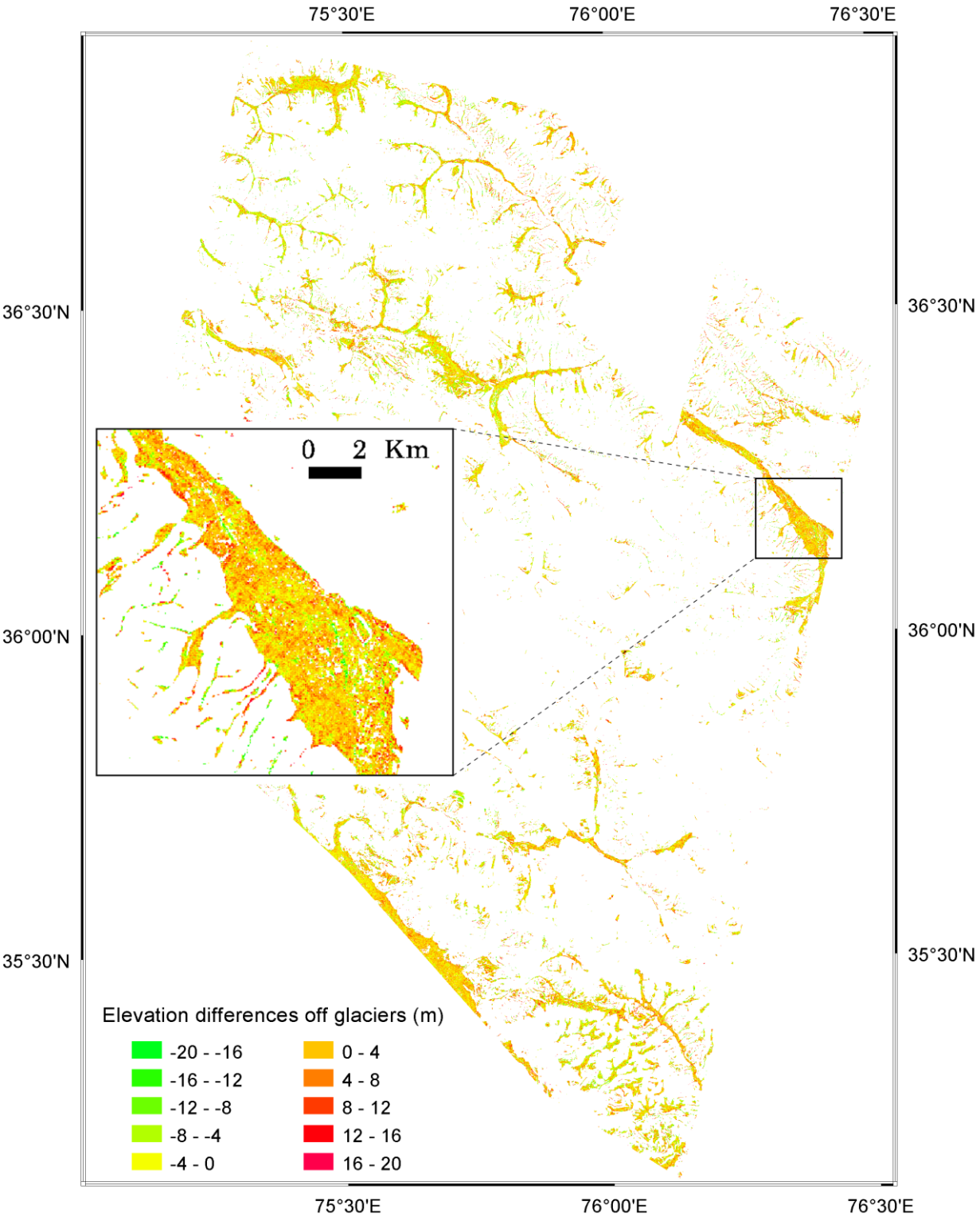


**Figure S4:** Map of elevation differences (SPOT5 – SRTM) over ice free terrain, between 2000 and 2008, after planimetric adjustment and removal of systematic elevation biases. The total ice free area is 1180 km².

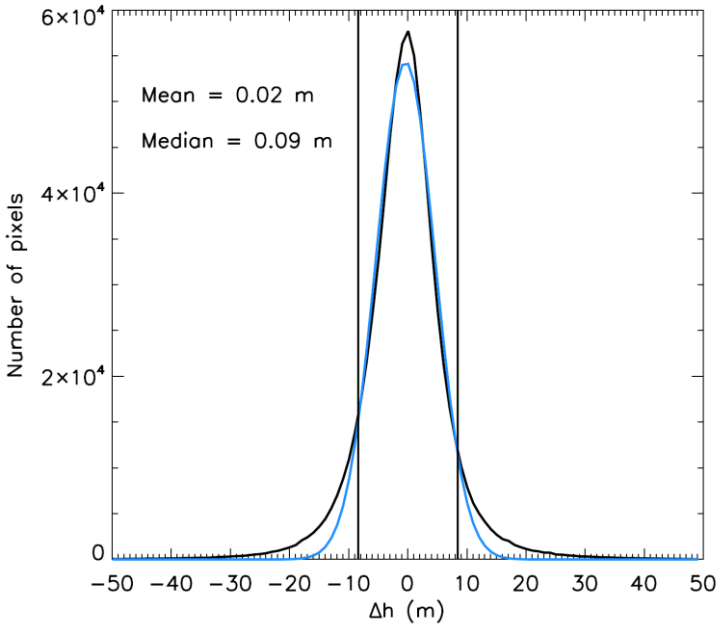


**Figure S5:** Distribution of elevation differences (black line) on the ice-free terrain after planimetric and vertical adjustment of the DEMs. The blue line represents the corresponding gaussian fit. The vertical lines represent the standard deviation of elevation differences (± 8.4 m).

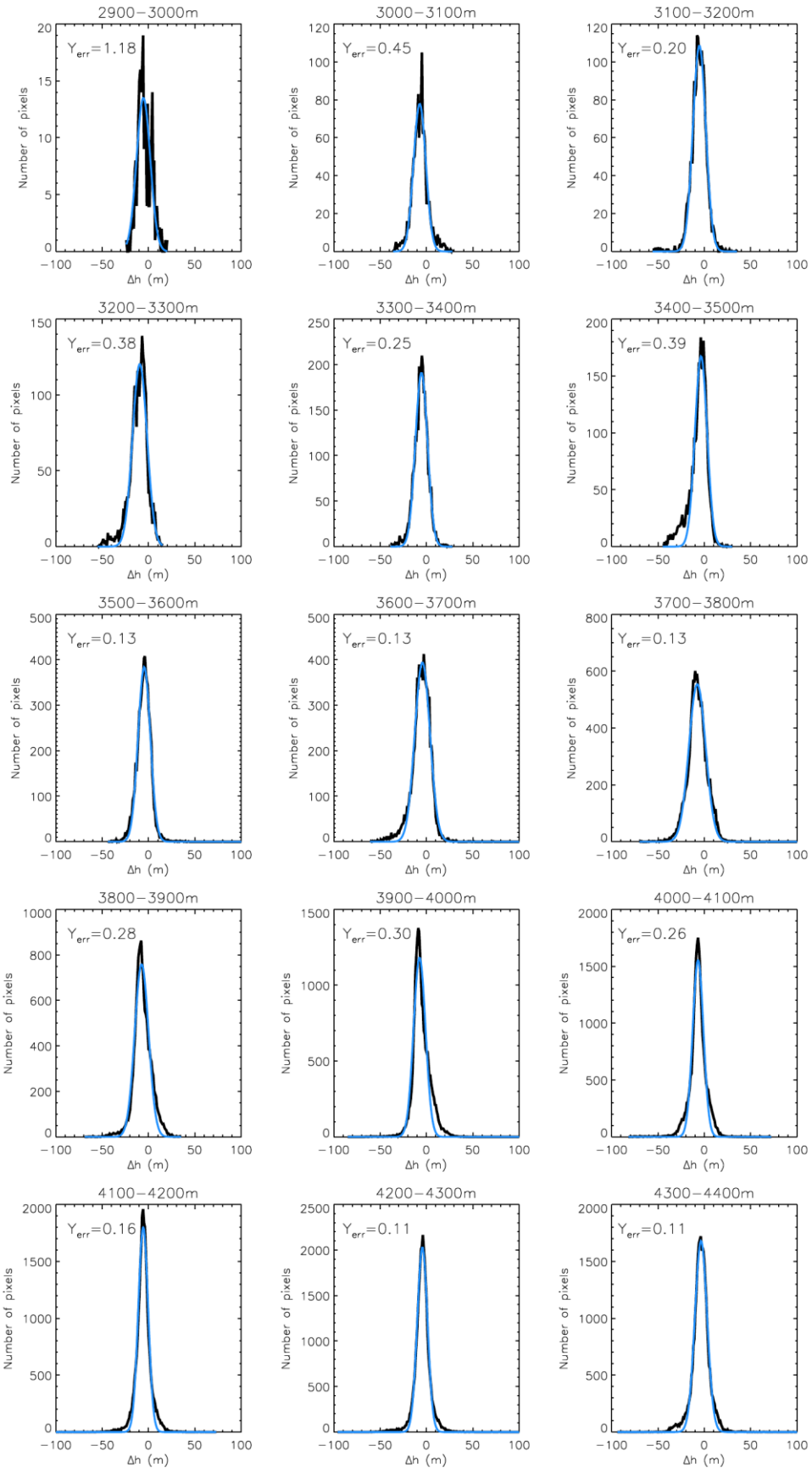

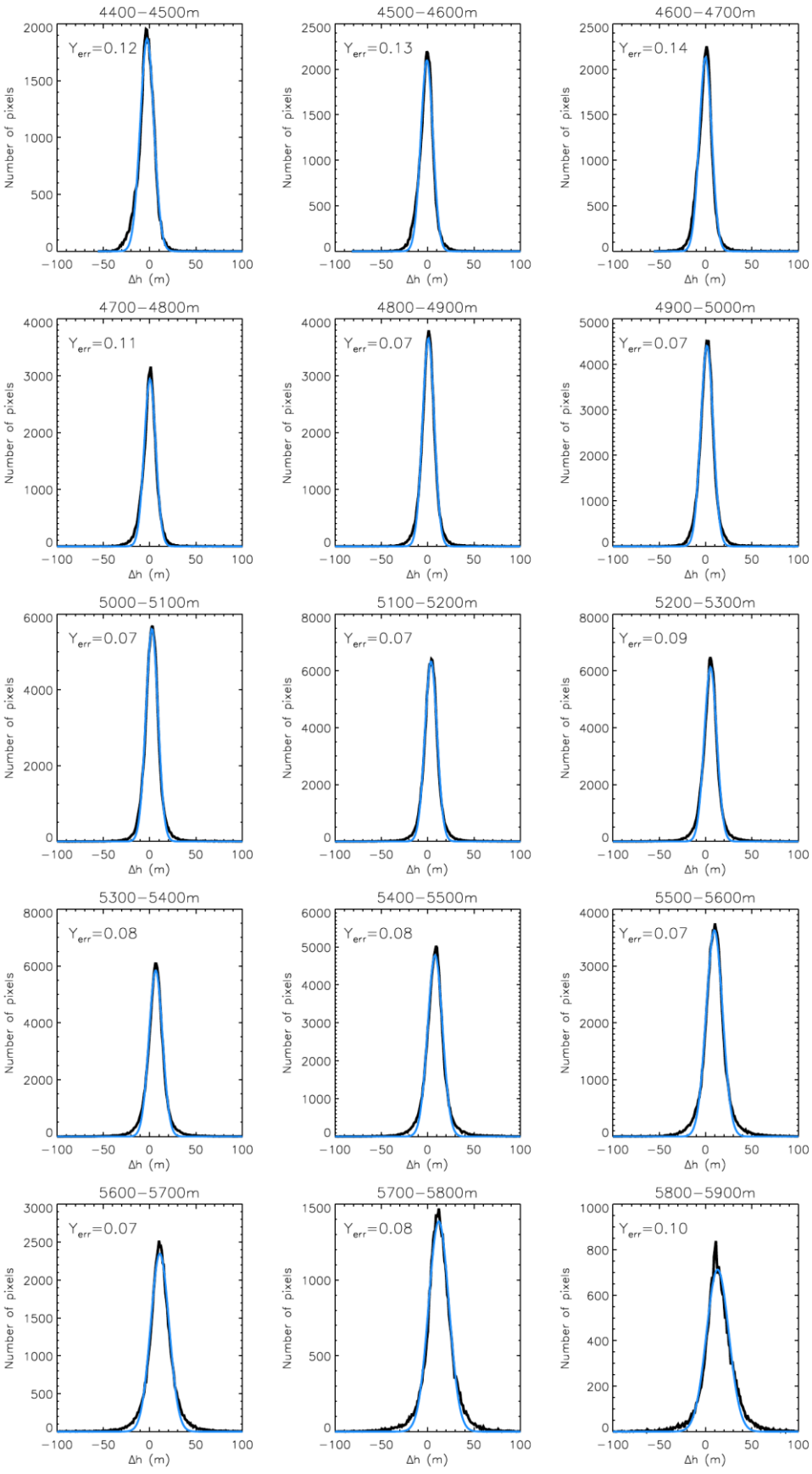

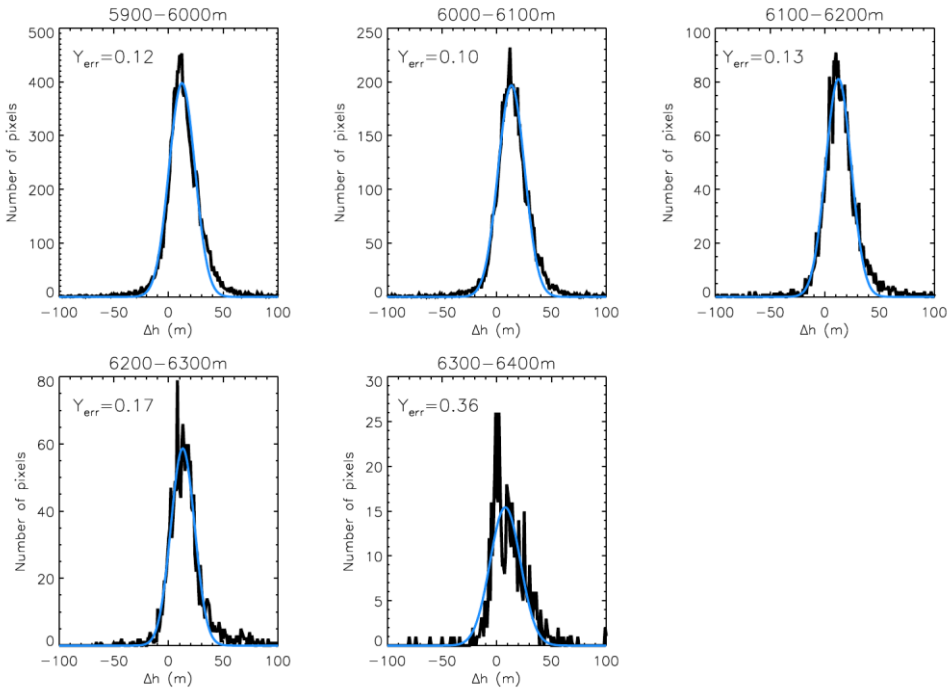


**Figure S6:** Distribution of elevation changes (black line) in each altitude interval, for non surging glaciers only. The blue line represents the corresponding gaussian fit. The standard error between the data and the model, normalized by the number of pixels of each interval ($Y_{err}$) is also given (in percent).

## Supplementary references


31. **Korona, J., Berthier, E., Bernard, M., Rémy, F. & Thouvenot, E.** SPIRIT. SPOT 5 stereoscopic survey of Polar Ice: Reference Images and Topographies during the fourth International Polar Year (2007-2009). *ISPRS J. Photogram.* **64**, 204-212 (2009).

32. **Rabus, B., Eineder, M., Roth, A. & Bamler, R.** The Shuttle Radar Topography Mission-a new class of digital elevation models acquired by spaceborne radar. *ISPRS J. Photogram*. **57**, 241-262 (2003).

33. **Rabatel, A., Dedieu, J. &Vincent, C.** Using remote-sensing data to determine equilibrium-line altitude and mass-balance time series: validation on three French glaciers, 1994-2002. *J. Glaciol.* **51**, 539-546 (2005).

34. **Nuth, C., *et al.*** Estimating the long term calving flux of Kronebreen, Svalbard, from geodetic elevation changes and mass balance modelling, *J. Glaciol.* **58**, 119–133 (2012).

35. **Leprince, S., Ayoub, F., Klinger, Y. & Avouac J.P.** Co-Registration of Optically Sensed Images and Correlation (COSI-Corr): an operational methodology for ground deformation measurements, *IEEE Trans. Geosci. Remote Sens.* **45**, 1529-1557 (2007).

36. **Nuimura, T., *et al.*** Temporal changes in elevation of the debris-covered ablation area of the Khumbu Glacier in the Nepal Himalaya since 1978, *Arc. Antarc. Alp. Res.* **43**, 246-255 (2011).

37. **Oerlemans, J., Giesen, R. & Van Den Broeke M.** Retreating alpine glaciers: increased melt rates due to accumulation of dust (Vadret da Morteratsch, Switerland), *J. Glaciol.* **55**, 729-736 (2009).

38. **Sakai, A., Nakawo, M. & Fujita, K.** Distribution characteristics and energy balance of ice cliffs on debris-covered glaciers, Nepal Himalaya, *Arc. Antarc. Alp. Res.* **34**, 12-19 (2002).

39. **Matsuo, K. & Heki, K.** Time-variable ice loss in Asian high mountains from satellite gravimetry. *Earth Planet. Sci. Lett.* **290**, 30-36 (2010).

40. **Jacob, T., Wahr, J., Pfeffer, W.T. & Swenson S.** Recent contributions of glaciers and ice caps to sea level rise. *Nature*, **482**, 514-518 doi:10.1038/nature10847 (2012).

41. **Bretherton, C., *et al.*** The effective number of spatial degrees of freedom of a time-varying field, *J. Clim.* **12**, 1990-2009 (1999).

42. **Goodchild, M.F.** Spatial Autocorrelation. Catmog 47, Geo Books. (1986).